Dielectric Permittivity and Relaxation of Electrolyte Solutions and their Solvents

J. Barthel and R. Buchner
Institute of Physical and Theoretical Chemistry, University of Regensburg, D-8400 Regensburg, Germany

1 Introduction

The understanding of the properties of liquid solutions involving ionic species is fundamental for many branches of basic research and technology, ranging from biology and geosciences to 'proper' chemistry, where many processes take place in aqueous and non-aqueous electrolyte solutions.[1-5] A wealth of information on solvents and solutions can be deduced from their response to time-dependent electric fields.

The investigation of dielectric relaxation yields valuable information on the structure and dynamics of liquid systems. The experimental technique to study these phenomena is fairly old and widely applied in solid state studies[6] and in the investigation of polymers[7] and meso-phases.[8] For a long time technical problems arising from the significantly higher frequencies needed for the investigation of liquid systems (giga-hertz compared to kilo- and mega-hertz in the aforementioned applications) prevented routine investigations on solutions.

This review will describe recent progress in the determination of precise data in the giga-hertz range resulting from the use of modern equipment. After an introduction of the theoretical background of dielectric relaxation spectroscopy (dielectrometry) and the presentation of the experimental techniques we will tie the results on electrolyte solutions into the framework of solution chemistry. Readers interested in the applications of dielectric relaxation spectroscopy in biophysics are referred to reference 9.

2 Principles and Concepts of Complex Permittivity Studies on Liquid Systems

The response of a dielectric medium of relative permittivity ϵ and specific conductance κ to the application of a time-dependent electric field $\vec{E}(t)$ is a current composed of an Ohmic contribution proportional to κ and of a displacement current caused by the polarization of the sample $\vec{P}(t)$. In non-conducting molecular liquids only polarization of the sample takes place

$$\vec{P} = \vec{P}_\mu + \vec{P}_\alpha = \epsilon_0(\epsilon - 1)\vec{E} \qquad (1)$$

with ϵ_0 as the permittivity of the vacuum. $\vec{P}(t)$ arises from two processes. The induced polarization $\vec{P}_\alpha(t)$ is due to the *intramolecular* charge separation by the action of the local internal electric field $\vec{E}_j^{\text{int}}$ on the polarizability α_j of molecule j and is given by equation 2a where V is the volume of the sample. Energy absorption by the molecule occurs at well-defined frequencies corresponding to *intramolecular* rotational and vibrational modes and to the excitation of electrons in resonant processes, controlled by quantum mechanics. The time constants of these processes are found in the femto-second range. They are very fast compared to the second polarization mechanism yielding the oriental polarization $\vec{P}_\mu(t)$.

$$\vec{P}_\alpha = \sum_j \frac{\alpha_j \vec{E}_j^{\text{int}}}{V} \qquad (2a)$$

$$\vec{P}_\mu = \sum_j \frac{\langle \vec{\mu}_j(t) \rangle}{V} = \sum_j \frac{(\vec{\mu}_j)^2}{3kTV} E_j^{\text{dir}} \qquad (2b)$$

When the oriental polarization $\vec{P}_\mu(t)$ is the result of the alignment of the permanent dipole moments $\vec{\mu}_j$ of the molecules in the local directing electric field $\vec{E}_j^{\text{dir}}$ against thermal motion it is given by equation 2b; the angular brackets denote the ensemble average. Other processes, such as kinetic processes, also may contribute as shown in Figure 1. The relation between the external field $\vec{E}$ and the local fields $\vec{E}_j^{\text{dir}}$ and $\vec{E}_j^{\text{int}}$ depends on the theoretical level adopted for the calculation of $\vec{P}$; for details see reference 10. The equilibrium value of $\vec{P}_\mu$, and especially the time-evolution for reaching it, are characteristic for *intermolecular* interactions. For a simple orientational process as given in Figure 2 the spectrum is governed by a dissipative process with energy absorption $\epsilon''(\nu)$ over a wide frequency range, accompanied by a dispersion $\epsilon'(\nu)$ of the permittivity ϵ. For liquids and solutions at room temperature the relaxation of $\vec{P}_\mu$ occurs in the nano-second to pico-second range which corresponds to frequencies in the microwave region (see Figure 1).

The independent decrease of induced and orientational polarization in different time scales allows the separation of $\vec{P}_\mu$ and $\vec{P}_\alpha$ by the introduction of the 'infinite-frequency' permittivity ϵ_∞, see Figure 2

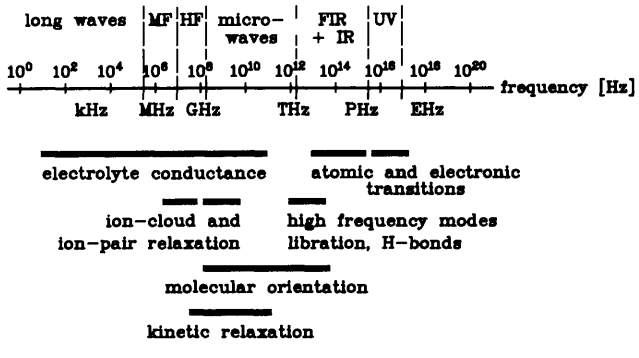

Figure 1 Frequency regions and respective processes contributing to the permittivity of liquids and solutions at room temperature.

Josef Barthel graduated from the University of Saarbrücken (1953) and studied with Professor J. E. Dubois, Paris, for his Ph.D. (1956) and Habilitation in Physical Chemistry (1959). From 1959 to 1971 he was Assistant Professor, Professor, and Head of the Electrochemistry Section at the University of Saarbrücken and Visiting Professor at the University Paris VII. Since 1971 he has held the chair of Physical Chemistry at the University of Regensburg. He is Director of the Institute of Physical and Theoretical Chemistry.

Richard Buchner graduated in 1982 from the University of Regensburg, where he also studied with Professor Barthel for his Ph.D. (1986). After one year as Post-doctoral Fellow with Dr. J. Yarwood at the University of Durham, U.K., he returned to Regensburg where he now has a position as Akad. Rat at the Institute of Physical and Theoretical Chemistry. His main research interest is the application of dielectric relaxation experiments to studies of the structure and dynamics of liquids and solutions.

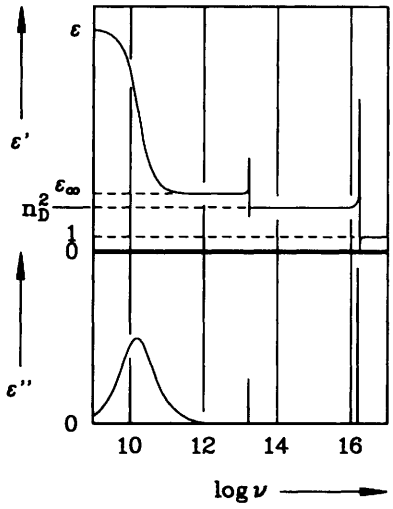

Figure 2 Schematic dielectric dispersion $\epsilon'(\nu)$ and loss $\epsilon''(\nu)$ spectra for a polar liquid with a single Debye relaxation process ($\tau \approx 10$ ps) in the microwave and two resonant transitions in the IR and UV range; n_D is the refractive index in the visible spectral range.

$$\vec{P}_\mu = \epsilon_0(\epsilon - \epsilon_\infty)\vec{E} \tag{3a}$$

$$\vec{P}_a = \epsilon_0(\epsilon_\infty - 1)\vec{E} \tag{3b}$$

Then it is possible to relate the dispersion amplitude $(\epsilon - \epsilon_\infty)$ of orientational polarization to the number density N_i and the dipole moment μ_i of species i. The Kirkwood–Fröhlich theory yields for pure liquids

$$g_K\mu^2 = \frac{9\epsilon_0 kT(\epsilon - \epsilon_\infty)(2\epsilon + \epsilon_\infty)}{N\ \epsilon(\epsilon_\infty + 2)^2} \tag{4}$$

where g_K is the Kirkwood factor, which is characteristic for the orientational correlation between the dipole molecules.

Two experimental approaches are possible with orientational polarization; the time domain and the frequency domain method. In a *time domain* experiment, a field jump is applied to the equilibrated sample at time $t_0 = 0$, where the orientational polarization is $\vec{P}_\mu^o$. Whereas $\vec{P}_a$ follows the polarity changes of the applied field without time delay, $\vec{P}_\mu$ approaches its new equilibrium $\vec{P}_\mu^\infty$ with a characteristic function $F_p^{or}(t)$, called the step response function

$$\vec{P}_\mu(t) = (\vec{P}_\mu^o - \vec{P}_\mu^\infty)F_p^{or}(t) + \vec{P}_\mu^\infty \tag{5a}$$

$$F_p^{or}(t) = \frac{\langle \vec{P}_\mu^o \cdot \vec{P}_\mu(t)\rangle}{\langle \vec{P}_\mu^o \cdot \vec{P}_\mu^o\rangle} \tag{5b}$$

It can be shown that $F_p^{or}(t)$ is the correlation function of the macroscopic dipole moment $\vec{M}_{or}(t) = \sum_j \vec{\mu}_j(t)$ and contains the entire information on the dynamics of all dipolar species in the solution.

Experience shows that around ambient temperature the long-time behaviour of many non auto-associating dipolar liquids is controlled by an exponential decay function, $F_p^{or}(t) = \exp(-t/\tau)$, with relaxation time τ. Associating liquids and mixtures exhibit more complex response functions which must be deconvoluted into normal modes. The short time behaviour of all liquids is more complex. The step response function $F_p^{or}(t)$ is characteristic for the reorganization of the phase structure of a macroscopic sample after a perturbation. The study of molecular processes and the comparison with results from other methods, such as computer simulation, NMR relaxation, Rayleigh or quasi-elastic neutron scattering requires microscopic correlation functions. An obvious choice for dielectric relaxation studies is the correlation function of the molecular dipole vector.

$$\phi(t) = \frac{\langle \vec{\mu}_j(t_0)\cdot\vec{\mu}_j(t)\rangle}{\langle \vec{\mu}_j(t_0)\cdot\vec{\mu}_j(t_0)\rangle} = \langle \cos\theta(t)\rangle \tag{6}$$

Possible cross-terms due to the correlation of two arbitary molecules j and k, *i.e.* $\langle \vec{\mu}_j(t_0)\cdot\vec{\mu}_k(t)\rangle \neq 0$, make the relation between $F_p^{or}(t)$ and $\phi(t)$ complicated. However, for an exponentially decaying orientational polarization of a pure dipolar fluid, $\phi(t)$ is also exponential and the corresponding molecular relaxation time τ' is linked[11] to the macroscopic relaxation time τ by

$$\tau' = \frac{2\epsilon + \epsilon_\infty}{3\epsilon} g_K \tau \tag{7}$$

When molecular reorientation is governed by random small angle motions of the dipole vector and hence is a rotation diffusion, the molecular relaxation time τ' can be linked to the sample viscosity η and the molecular volume V_m of the rotating particle with the help of an empirically modified Stokes–Einstein–Debye equation[12]

$$\tau' = \frac{3V_m}{kT} f_\perp C\eta \tag{8}$$

The parameter $f_\perp$ is related to the ratio of the principal axes of the rotational ellipsoid representing the molecule and the empirical factor C couples the microscopic viscosity felt by the rotating entity to macroscopic viscosity; C equals unity for stick boundary conditions. For isotropic rotational motions of a molecule theory predicts

$$\tau' = \tau_{QENS} = 3\tau_{NMR} = 3\tau_{Ray} = 3\tau_{Ram} \tag{9}$$

τ_{QENS}, τ_{NMR}, τ_{Ray}, and τ_{Ram} are the molecular rotational correlation times of quasi-elastic neutron scattering, nuclear magnetic resonance, Rayleigh and Raman spectroscopy, respectively. In contrast, for relaxation mechanisms governed by discrete jumps, such as those involving chemical reactions, the correlation times of equation 9 are approximately equal. For a detailed discussion of such microscopic relaxation models see references 10 and 13.

In the *frequency domain* the system response to the application of a harmonic field, $\vec{E}(t) = \vec{E}_0 \exp(i\omega t)$, of frequency ν ($\omega = 2\pi\nu$) is probed. With increasing frequencies a situation is reached where the polarity change of the applied electric field prevents the sample from reaching equilibrium. The accompanying energy dissipation yields amplitude reduction and phase shift of the propagating wave and consequently also of the frequency-dependent orientational polarization. A convenient way to describe both effects is the introduction of the frequency-dependent complex permittivity $\hat{\epsilon}(\omega) = \epsilon'(\omega) - i\epsilon''(\omega)$, where the dielectric dispersion $\epsilon'(\omega)$ is a measure for $\vec{P}_\mu(\omega)$ and the dielectric loss $\epsilon''(\omega)$ is a measure for the energy absorption of the sample, as sketched in Figure 2. The complex relative permittivity $\hat{\epsilon}(\omega)$ is related to the negative time-derivative of the step response function $F_p^{or}(t)$ *via* the Laplace transformation

$$\hat{\epsilon}(\omega) = (\epsilon - \epsilon_\infty)\int_0^\infty \left(-\frac{\partial F_p^{or}(t)}{\partial t}\right) e^{-i\omega t} dt \tag{10}$$

A single first-order polarization decay with $F_p^{or}(t) = \exp(-t/\tau)$ yields the well-known Debye formulae

$$\epsilon'(\omega) = \epsilon_\infty + \frac{\epsilon - \epsilon_\infty}{1 + \omega^2\tau^2} \tag{11a}$$

$$\epsilon''(\omega) = \frac{(\epsilon - \epsilon_\infty)\omega\tau}{1 + \omega^2\tau^2} \tag{11b}$$

where the characteristic frequency $\nu_c = (2\pi\tau)^{-1}$ defines the point of inflexion of the dispersion curve and the maximum of the loss spectrum, see Figure 2. A plot of $\epsilon''(\omega)$ *vs.* $\epsilon'(\omega)$, the so-called Argand diagram, yields a semi-circle with its centre on the ϵ'-

axis. Generally more than one relaxation process takes place in a solution and it may be appropriate to use empirical relaxation-time distribution functions, such as the Cole–Cole ($0 \leqslant \alpha < 1$, $\beta = 1$) or the Cole–Davidson ($\alpha = 0$, $0 < \beta \leqslant 1$) to fit the individual processes

$$\hat{\epsilon}(\omega) = \epsilon_\infty + (\epsilon - \epsilon_\infty) \sum_{j=1}^{n} \frac{g_j}{[1 + (i\omega\tau_j)^{1-\alpha_j}]^{\beta_j}} \qquad (12a)$$

In equation 12a n separable processes j contribute with relaxation times τ_j and relative dispersion amplitudes

$$g_j = \frac{\epsilon_j - \epsilon_{\infty j}}{\epsilon - \epsilon_\infty}, \quad \epsilon_{\infty j} = \epsilon_{j+1} \qquad (12b,c)$$

to the total dispersion reaching from the static value $\epsilon = \epsilon_1$ to ϵ_∞. The parameters $\alpha_j > 0$ and $\beta_j < 1$ describe a symmetric or asymmetric distribution of relaxation times for process j, respectively.

At frequencies below 300 to 500 GHz it is always possible to fit the experimental data to such models. A major problem in the choice of the appropriate model is the limited frequency coverage of the experimental data. For example, early data for methanol, covering $0.95 \leqslant \nu/\mathrm{GHz} \leqslant 12$, suggested a single process with Cole–Cole distribution, whereas the now available data between 0.95 and 300 GHz require the separation of 3 Debye processes.[14]

A different approach to the description of dielectric relaxation based on the mesoscopic model of Dissado and Hill[15] permitting the reproduction of a wide range of band shapes, has been successfully used to fit the data of undercooled liquids, polymers, and solids. The model assumes that condensed state materials are composed of spatially limited regions with partially regular structural order and strongly coupled motions of the constituents, modulated by the weakly coupled inter-cluster motions and interactions responsible for the long-range structure. In this theory the complex permittivity spectrum is given by the relation

$$\hat{\epsilon}(\omega) = \epsilon_\infty + \frac{\epsilon - \epsilon_\infty}{F(0)} \frac{1}{(1 + i\omega\tau)^{1-n}} \times {}_2F_1\left(1 - n, 1 - m; 2 - n; \frac{1}{1 + i\omega\tau}\right) \qquad (13)$$

with $0 < m,n < 1$; ${}_2F_1(,;;)$ is the Gaussian hypergeometric function with $F(0) = {}_2F_1(1 - n, 1 - m; 2 - n; 1)$ as the zero frequency limit. Empirically, n and $1 + m$ ($0 < n,m \leqslant 1$) can be identified with the exponents x of the power-laws, $\exp[-(t/\tau)^x]$, often observed as the short- and long-time asymptotic limits of $F_p^{or}(t)$.

3 Experimental Techniques and Problems

The experimental techniques of the frequency and time-domain methods yield, more or less implicitly, the complex propagation constant of the electromagnetic wave in the sample, $\hat{\gamma}(\omega) = \alpha + i\beta$, which compares the amplitude and the phase of the field $\vec{E}(z)$ propagating in z-direction at point z to the field $\vec{E}_0$ at a reference point $z_0 = 0$

$$\vec{E}(z) = \vec{E}_0 \exp(-\hat{\gamma}z) \qquad (14)$$

In equation 14, α is the attenuation coefficient and $\beta = 2\pi/\lambda_s$ is the phase constant; λ_s is the wavelength in the sample. Only recent developments used for the investigation of electrolyte solutions and their solvents will be considered here; a general introduction into the principles of experimental techniques is given in reference 9.

A fundamental problem for all methods when used in the study of conducting samples is the fact that only the sum of displacement and Ohmic current can be experimentally determined. Since *a priori* both complex permittivity $\hat{\epsilon}(\omega)$ and specific conductance $\hat{\kappa}(\omega)$ are frequency dependent, assumptions must be made to split the measured generalized complex permittivity $\hat{\eta}(\omega)$

$$\hat{\eta}(\omega) = \hat{\epsilon}(\omega) + \frac{i\kappa(\omega)}{\omega\epsilon_0} \qquad (15)$$

There is evidence that the dispersion of conductivity is small in comparison to the experimental accuracy of $\hat{\eta}(\omega)$ in the microwave range. It is therefore generally accepted to assume frequency-independent conductivities with $\kappa'(\omega) = \kappa$ and $\kappa''(\omega) = 0$, where κ is the specific conductance of the sample at quasi-static frequencies, so that

$$\eta'(\omega) = \epsilon'(\omega); \quad \eta''(\omega) = \epsilon''(\omega) + \frac{\kappa}{\omega\epsilon_0} \qquad (16a,b)$$

Figure 3 shows the loss spectrum of a 0.36 molar aqueous $MgSO_4$ solution with [$\eta''(\nu)$, curve 1] and without [$\epsilon''(\nu)$, curve 2] conductivity contribution. Obviously the Ohmic loss dominates at low frequencies and although η'' can be determined with an accuracy of 1—3% and κ is even more precise, ϵ'' and its error may have equal order of magnitude for highly conducting solutions at low frequencies.

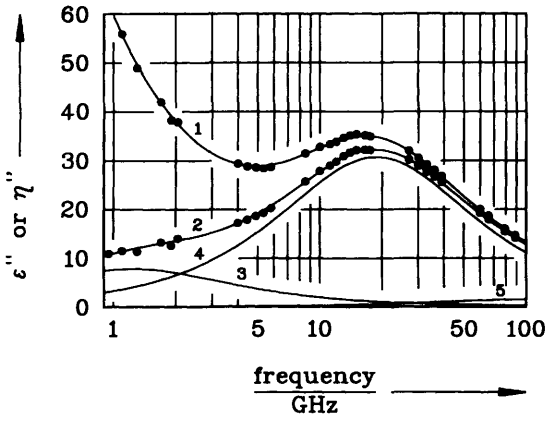

Figure 3 Experimental data (●) and calculated total loss (η'', curve 1) and dielectric loss spectrum (ϵ'', curve 2) of an aqueous $MgSO_4$ solution ($c = 0.3634$ mol dm^{-3}; $\kappa = 2.7163\Omega^{-1}$ m^{-1}) at 25 °C fitted with a superposition of 3 Debye relaxation processes. Also shown are the individual contributions of the ion-pair (curve 3), and of the slow and fast water relaxation process (curves 4,5).

For the commonly used electrolyte solutions the dispersion of solvent and solution permittivities takes place in the microwave region at frequencies between 50 MHz and 500 GHz. Unfortunately, the coverage of this spectral range is not possible with a single instrument because the wavelength λ of the electromagnetic radiation is comparable to the dimensions of the measuring equipment; frequencies of $\nu = 1$ GHz and $\nu = 100$ GHz correspond to $\lambda = 30$ cm and $\lambda = 0.3$ cm, respectively. This restricts the application of free-space methods, common for infrared and optical spectroscopy, to frequencies above 100 GHz. Below about 20 GHz coaxial transmission lines allow broad-band experiments, but the remaining frequency gap must be covered with the help of conventional microwave equipment based on hollow metallic waveguides, usually of rectangular cross section ($a \times b$), which are usuable only in a limited fequency band.

Transmission line theory shows that for a waveguide of specified geometry an infinite series of solutions exists for the propagation of a wave having free-space wavelength λ. They can be classified into TE-modes having no component of the electric field in the direction of propagation, z, and into TM-modes with no magnetic component in z-direction. Each mode is characterized by a specific propagation constant $\hat{\gamma}$ and by a cut-off wavelength λ_c which defines the lowest frequency able to pass the waveguide with the corresponding field type. The fundamental

mode, TE_{10}, has the largest possible cut-off wavelength, $\lambda_c(TE_{10}) = 2a\sqrt{\mu\epsilon}$ for a loss-free dielectric of permittivity ϵ and permeability μ. TE_{10} can propagate in a frequency region where it is the only stable field type and higher order modes are damping out rapidly. Technical reasons restrict this frequency band to $0.53 \leqslant \lambda/\lambda_c(TE_{10}) \leqslant 0.8$ for the geometry $a = 2b$. For the air-filled waveguide operated in the frequency range of the TE_{10}, higher order modes, which may be excited at any irregularity of the waveguide system, are not relevant. However, in the part of the waveguide serving as the measuring cell they may propagate due to $\epsilon' \gg 1$ and thus distort the results. The influence of higher order modes can only be minimized by careful cell design and construction. With this problem solved, however, waveguide equipment produces data of high accuracy for high loss liquids such as electrolyte solutions. Figure 4 shows a block diagram of the E-band apparatus (60—90 GHz) of our laboratory which is one of the five waveguide measuring lines needed to cover the frequency range from 4 to 89 GHz. For a detailed description we refer to the original publication.[16]

The method of travelling waves requires only relative measurements of signal amplitude and probe position. It yields $\hat{\gamma}$ in a transmission experiment where the waveguide part of the instrument, numbers 1—9, forms an interferometer with the cell C and movable probe P in one beam. The cell is a piece of standard waveguide sealed at one end with a thin mica window. The probe is a gold-plated ceramics bar of cross-section adjusted to its permittivity. It can be moved with a resolution of 0.1 μm. The attenuation coefficient α is obtained by measuring the transmitted power as a function of probe position z with closed reference beam (1b, 9, 1c). To obtain λ_s amplitude and phase of sample and reference beam are balanced at a set probe position with the help of the attenuators 1b, 9, 1c and the phase shifter 4 to obtain destructive interference, and then the probe is moved until the next interference minimum is found. For the TE_{10}-mode $\hat{\eta}$ is given by

$$\eta'(\nu) = \left(\frac{c_0}{\nu}\right)^2 \left[\left(\frac{1}{\lambda_s}\right)^2 - \left(\frac{\alpha}{2\pi}\right)^2 + \left(\frac{1}{2a}\right)^2\right] \tag{17a}$$

$$\eta''(\nu) = \left(\frac{c_0}{\nu}\right)^2 \cdot \frac{\alpha}{\pi\lambda_s} \tag{17b}$$

Figure 4 Block diagram of the E-band apparatus (60–90 GHz): 1—9 wave-guide interferometer with cell C and movable probe P; PLO, PLO-D, PLO-P, microwave signal source and control unit; 8, MMC, S, RE, signal detection unit; HH, MT, SMD, SM, PM, SP, probe position control unit; PD, interface unit enabling the control of four bands (E, A, Ku, X) in the frequency range 12 to 90 GHz; MC microcomputer. For details see reference 16.

with c_0 as the speed of light and α determined with the unit of [Np m^{-1}]. The accuracy which can be achieved with this equipment is better than 1.5% in ϵ' and 2.5% in ϵ'' for frequencies up to 40 GHz and approximately 3% both in ϵ' and ϵ'' above 40 GHz.

An alternative approach for the determination of $\hat{\eta}(\omega)$ of lossy liquids are reflection experiments. Recently, Sheppard and co-workers[17] developed waveguide systems covering 29 GHz to 90 GHz which yield a precision comparable to the travelling wave equipment described above. Here the complex propagation coefficient $\hat{\gamma}$ is related to the power $P(z)$ reflected from the sample-filled cell short-circuited by a movable plunger at the plunger position z as

$$P(z) = \left| \frac{R_1 + R_2 \exp(-2\hat{\gamma}z)}{1 + R_3 \exp(-2\hat{\gamma}z)} \right|^2 \tag{18}$$

where R_1 is a real constant and R_2 and R_3 are complex constants.

In the far infrared region, above 90 GHz (3 cm^{-1}), the necessary machining tolerances for high accuracy data are prohibitive for the construction of waveguide equipment, but it is possible to use free-space propagation with mirrors, lenses, *etc.* which allow broad band experiments.[18] For different reasons, but especially because of the lack of powerful radiation sources, experiments are still difficult to perform so that actually only few data on pure liquids exist and almost no information is available on electrolyte solutions. This must be regretted, since not only the short-time motions of the solvent, which are very sensitive to the intermolecular interaction potential, are probed in this spectral region, but also valuable information on ion–ion and ion–solvent dynamics is expected from the libration modes of the ion pair in the cage of surrounding solvent molecules. Hopefully, this situation will change now with the appearance of bright synchotron radiation sources, recently used to determine the optical constants of pure acetonitrile between 20 cm^{-1} and 250 cm^{-1} over a large temperature range.[19]

Coaxial lines, which consist of a hollow outer conducter and a centred inner conductor with radii a and b, and separated by a dielectric which may be the sample, impose no principal limitation on the band width, but problems of cell construction actually still restrict complex permittivity measurements to frequencies below about 20 GHz. As for waveguides, transmission and reflection methods are realized, but here additionally to frequency domain techniques, time domain experiments are possible. The accuracy of these methods largely depends on the properties of the system studied and on the experience of the experimenter to choose the appropriate method and correction routine; for not too highly conducting electrolyte solutions 1—2% in η' and η'' are possible.

In the frequency domain, commonly variable path-length

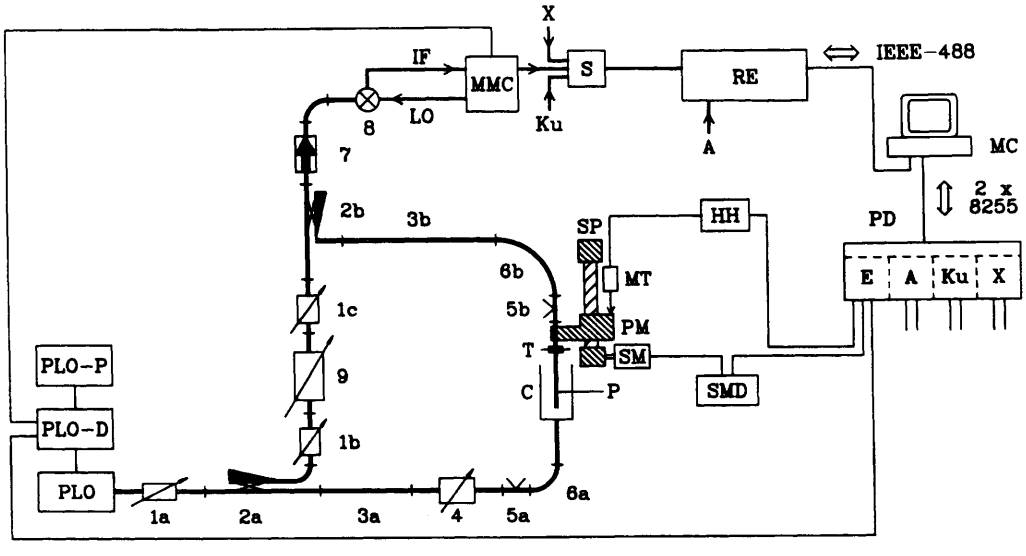

cells are used for reflection or transmission experiments.[9] They only require amplitude detection, but the realizable cell length sets a low frequency limit for the determination of λ_S. An elegant possibility to circumvent this problem is the simultaneous measurement of amplitude and phase in a fixed path-length cell with the help of vector network analysers now able to reach 20 GHz with sufficient precision;[20] $\hat{\gamma}$ is obtained from a comparison of the empty cell and the sample data.

Transmission cells can also be used for reflection experiments, but special cut-off cells are more advantageous for this type of experiment. Here the signal reflected from an open-ended line immersed in the solution is recorded.

In principle the same type of cells and a similar experimental arrangement can be used for time domain experiments. The principles of this method are given in reference 9. Here a fast rising voltage step is applied to the cell and the transmitted or reflected signal is recorded as a function of time. The distortion of the pulse arises from the finite response time of the sample-filled cell, essentially determined by the step response function $F_p^{or}(t)$. Actually the finite rise-time of the equipment limits the frequency range to $\nu < 10$ GHz, but the method allows the determination of the complex permittivity spectrum down to several megahertz within a few minutes. It also needs only small sample volumes and has no movable parts which facilitates the investigation of temperature-dependent permittivity. A problem, however, are multiple reflections within the cell and spurious signals arising from line discontinuities outside, and a great deal of work has been dedicated to develop calibration procedures and correction routines for the various cell types.[21]

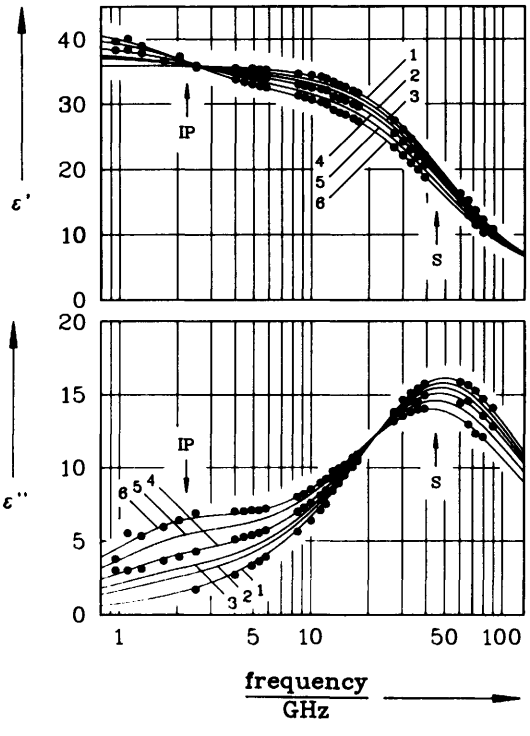

Figure 5 Real (a) and imaginary part (b) of the complex permittivity of LiBr solutions in acetonitrile at 25°C. 1: pure solvent; 2: 0.107 mol dm^{-3}; 3: 0.194 mol dm^{-3}; 4: 0.303 mol dm^{-3}; 5: 0.479 mol dm^{-3}; 6: 0.657 mol dm^{-3}. S and IP indicate the frequency regions of the relaxation processes of solvent and solute, respectively. For the sake of clarity experimental data (•) are only added for curves 1, 4, and 6.

4 The Influence of Electrolytes on the Dielectric Properties of the Solvent

Figure 5 shows a typical example of the effects produced by an electrolyte on the complex permittivity spectrum of the solution. The $\hat{\epsilon}(\omega)$ data of pure acetonitrile can be fitted with a Cole–Cole equation $\epsilon_S = 35.96$, $\tau_S = 3.21$ ps, $\epsilon_\infty = 2.26$, $\alpha_S = 0.028$: curve 1).

At increasing electrolyte concentration the amplitude of the solvent relaxation process (S in Figure 5) is reduced. Whereas ϵ_∞ is constant within experimental accuracy, ϵ_S drops to a value of 32.45 for the 0.657 molar solution, which is close to the saturation limit. Also a small low-frequency shift and broadening of the relaxation time distribution is observed, yielding $\tau_S = 3.67$ ps and $\alpha_S = 0.059$ at the highest concentration. Additionally a Debye-type dispersion step, increasing with electrolyte concentration, emerges at low frequencies around 2 GHz (IP in Figure 5). This process is attributed to the formation of dipolar ion pairs. It overcompensates the decrease of ϵ_S so that the static permittivity of the solution, ϵ, reaches $\epsilon = 41.88$ at the highest concentration.

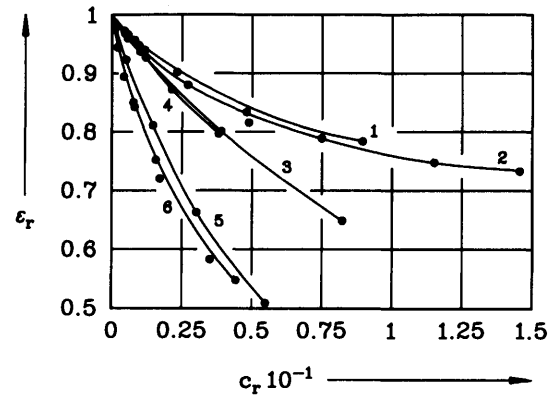

Figure 6 Relative static permittivity of the solvent, $\epsilon_r = \epsilon_S(c)/\epsilon_S(0)$, as a function of the relative concentration, $c_r = c/c_s$, of $NaClO_4$ at 25 °C in 1:acetonitrile; 2: propylene carbonate; 3: *N*,*N*-dimethylformamide; 4: formamide; 5: methanol; 6: *N*-methylformamide. c_s is the concentration of the solvent.
(From reference 14.)

4.1 Concentration Dependence of the Static Permittivity of the Solvent – a Probe for Ion–Solvent Interactions

Typical for electrolyte–solvent interactions is the dielectric depression, $\Delta\epsilon = \epsilon_S(0) - \epsilon_S(c)$, of the equilibrium solvent permittivity, ϵ_S. Dipolar aprotic solvents, such as acetonitrile (curve 1 in Figure 6) or propylene carbonate (2), are much less affected than liquids forming hydrogen-bonded chains, such as methanol (5) or *N*-methylformamide (6). The curves $\epsilon_S = f(c)$ usually are fitted to a polynomial of the type

$$\epsilon_S(c) = \epsilon_S(0) - \delta_\epsilon \cdot c + \beta_\epsilon \cdot c^n; \quad n = 3/2 \text{ or } 2 \qquad (19)$$

Values of δ_ϵ and β_ϵ for various electrolytes and solvents are reported in reference 22. The limiting slope at vanishing concentration is the dielectric decrement. Dielectric depression originates from a superposition of three effects. The dilution of the polar solvent by the dissolved apolar ($\epsilon \approx 2$) ions is a *volume effect* (Φ) which may become important for salts with large, weakly interacting ions, *e.g.* tetraalkylammonium perchlorates. *Irrotational bonding* (IB) of solvent molecules is mainly due to electrostatic interactions. The high field strength at the surface of the ion at least partly fixes the orientation of the surrounding solvent dipoles. Irrotational bonding incorporates non-coulombic ion–solvent interactions and may extend beyond the first solvation shell. Φ and IB reflect the structure of the solution. The third effect is of dynamic origin. The ion moves against the direction into which the solvent dipoles are oriented in the external field, creating thus a frictional force which lowers the mobility of the ion (dielectric friction) and decreases the permittivity of the solvent. According to Hubbard[23] and Onsager this *kinetic depolarization* (KD) is proportional to conductivity, κ, and is determined by the relaxation parameters of the pure solvent, $\epsilon_S(0)$, $\tau_S(0)$, and $\epsilon_\infty(0)$

$$\Delta\epsilon_{KD} = \xi \cdot \kappa; \quad \xi = p \cdot \frac{\epsilon_s(0) - \epsilon_\infty(0)}{\epsilon_s(0)} \cdot \frac{\tau_s(0)}{\epsilon_0} \tag{20}$$

The parameter p depends on the hydrodynamic boundary conditions for slip ($p = 2/3$) or stick ($p = 1$) ionic movement. A linear relation between κ and $\Delta\epsilon$ is often observed up to high concentrations but theoretical and experimental slope are not compatible; the theoretical depolarization factor ξ in equation 20 does not specifically depend on the electrolyte, in contrast to the experiment. To overcome this problem Hubbard, Colonomos, and Wolynes[23] suggested a molecular theory which predicts a strong dependence of ξ on the ionic radius and yields the slip result of equation 20 as the limiting case for large ions.

Actually no unifying theory exists which incorporates the aforementioned contributions to the dielectric depression $\Delta\epsilon$ in a consistent way and which can be applied to finite concentrations of an electrolyte in any solvent. In our experience it is possible to analyse experimental decrements δ_ϵ by assuming that at the limit of infinite dilution volume effect, kinetic depolarization, and irrotational bonding are additive

$$\delta_\epsilon = \delta_\Phi + \delta_{IB} + \delta_{KD} = \delta_\epsilon^{eq} + \delta_{KD} \tag{21}$$

where $\delta_{KD} = \lim_{c\to 0} \Delta\epsilon_{KD}$ given by equation 20 with slip boundary conditions ($p = 2/3$). With this approach effective solvation numbers Z_{IB} are obtained from the equilibrium contribution to the decrement δ_ϵ^{eq}

$$Z_{IB} = (\delta_\epsilon^{eq} \cdot L - \Phi_V^0)\frac{\rho_0}{M_s} \tag{22a}$$

where

$$L = \frac{2\epsilon_s^2(0) + \epsilon_\infty^2(0)}{\epsilon_s(0)[\epsilon_s(0) - \epsilon_\infty(0)][2\epsilon_s(0) + \epsilon_\infty(0)]} \tag{22b}$$

In equation 22a ρ_0 is the density of the pure solvent and M_s is its molar mass; Φ_V^0 is the apparent partial molar volume of the solute at infinite dilution accessible from density data.

For electrolyte solutions of methanol and water sufficient information is available to split Z_{IB} into ionic contributions. As expected, the numbers of irrotationally bound solvent molecules differ from the number of molecules in the first solvation shell such as obtained from X-ray, neutron scattering, or molecular dynamics simulations, but are compatible with effective solvation numbers from solvation entropies or ionic mobilities.[14,24]

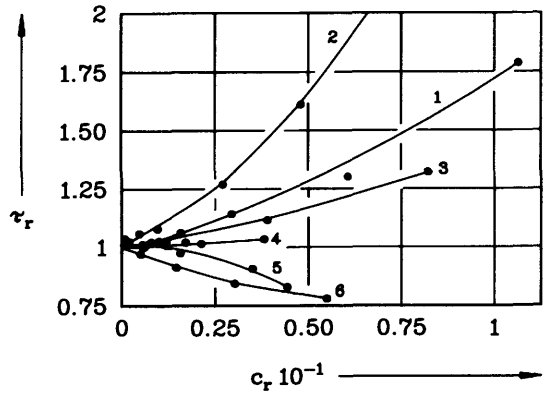

Figure 7 Relative relaxation times of the low-frequency dispersion step of the solvent, $\tau_r = \tau_{s1}(c)/\tau_{s1}(0)$, as a function of the relative concentration, $c_r = c/c_s$, of $NaClO_4$ at 25 °C in 1: acetonitrile; 2: propylene carbonate; 3: *N,N*-dimethylformamide; 4: formamide; 5: methanol; 6: *N*-methylformamide.
(From reference 14.)

4.2 Solvent Dynamics and Solvation Processes

Dipolar aprotic liquids are commonly characterized by a single dispersion step with relaxation time distribution, originating from the tumbling motion of the molecular dipoles. Hydrogen bonding liquids exhibit a more complex behaviour and the superposition of individual relaxation processes is required to reproduce the experimental complex permittivity spectrum. The dominating low-frequency relaxation process is too slow to be compatible with the reorientation of individual molecules; its relaxation time, τ_{s1}, probes a cooperative process of the H-bonded system, which also explains why the static permittivity ϵ_s is sensitive to the addition of ions, see Figure 6. The monoalcohols able to form wound chains of hydrogen-bonded molecules typically exhibit three dispersion steps which – in the order of decreasing relaxation time – are attributed to the probability of interaction between different chains, to the rotation of monomers and (predominantly) molecules situated at chain ends, and to a hindered 120°-rotation of alcohol molecules within the H-bonding system.[25] A similar behaviour is also found for NMF. Liquids able to form H-bonded networks, such as water, formamide, or diols, exhibit only two processes, because here the rotation of individual molecules and the rate of interaction of H-bonded clusters cannot be distinguished. The relaxation time of the high frequency dispersion of these liquids is close to the life-time of a hydrogen bond, but it does not probe the breaking of this bond in a translational motion; probably again it is characteristic for a partial rotation. Relaxation parameters of some solvents are given in Table 1; a more comprehensive list is given in reference 22.

Figure 7 shows the influence of $NaClO_4$ on the relaxation time τ_{s1} of the low-frequency dispersion step of various solvents. The comparison is facilitated by scaling the ordinate to relative electrolyte concentrations $c_r = c/c_s$; c_s is the concentration of the solvent in the solution. Obviously the relaxation time of non-hydrogen bonding liquids acetonitrile (curve 1), propylene carbonate (2), and *N,N*-dimethylformamide (3) increases and follows at least up to concentrations $c \approx 0.5$ mol dm^{-3} the increase of solution viscosity according to equations 7 and 8. The coupling factor C of equation 8 is generally smaller than unity and depends on the electrolyte, suggesting the conclusion that the rotational motion of the solvent molecules is less affected by ion–solvent interactions than translational motions. NMF (curve 5) and methanol (6) forming H-bonded chains, show a different behaviour. Although η also increases with electrolyte concentration the relaxation time of the first dispersion step, τ_{s1}, decreases. Here ion–solvent interactions, predominantly with Na^+, produce the breakdown of the solvent structure, also evidenced by the dramatic decrease of the static permittivity ϵ_s, *cf.* Figure 6, curves 5 and 6. Hydrogen-bonding solvents exhibit an electrolyte specific concentration dependence of τ_{s1} which reaches from a steady increase ($CdCl_2$ in water) over a pronounced maximum (tetrabutylammonium perchlorate in methanol) to monotonous decrease ($NaClO_4$ in NMF).

The influence of solvent dynamics on chemical reactivity of dissolved species has attracted interest in various fields.[26,27] Actually, the dynamics of solvation and the rates of hetero-

Table 1 Relaxation parameters of some liquids at 25 °C (From reference 21)

Compound	ϵ	τ_{s1} /ps	ϵ_2	τ_{s2} /ps	ϵ_3	τ_{s3} /ps	ϵ_∞
water	77.97	8.27	6.18	1.02	—	—	4.59
methanol	32.50	51.5	5.91	7.09	4.90	1.12	2.79
ethanol	24.32	163	4.49	8.97	3.82	1.81	2.69
formamide	108.8	37.3[a]	7.08	1.16	—	—	4.48
NMF	183.3	128	6.13	7.93	4.60	0.78	3.20
acetonitrile	35.96	3.21[b]	—	—	—	—	2.26
DMSO	46.40	20.5[c]	—	—	—	—	4.16

[a] $\alpha_1 = 0.0057$. [b] $\alpha_1 = 0.028$. [c] $\beta_1 = 0.888$.

genous and homogenous electron transfer reactions cannot yet be directly studied by dielectrometry, but theory and experiment show that the dielectric relaxation parameters of the solvent are of fundamental importance. For electron transfer (ET) reactions the measured rate constant k_{obs} can be expressed by the relation

$$k_{obs} = K_p \kappa_{el} \nu_n \exp[-(\Delta G^*_{os} + \Delta G^*_{is})/RT] \quad (23)$$

where K_p is the equilibrium constant for the formation of the precursor state prior to ET, κ_{el} is the electronic transmission coefficient, ν_n is the nuclear frequency factor. ΔG^*_{os} and ΔG^*_{is} are the outer-shell (solvent) and inner-shell (bond distortion) activation barriers of the reaction. The influence of the solvent on the reaction rate emerges from the frequency factor ν_n and the outer-shell barrier ΔG^*_{os} which both depend on the frequency-dependent dielectric properties of the solvent.

5 Solute Relaxation Processes – a Probe for the Study of Ion-Pairing and Complex Formation

The appearance of a solute relaxation process on the low frequency side of the complex permittivity spectrum is a common feature for solutions of 1:1 electrolytes in medium to low permittivity solvents, *cf.* the example LiBr/acetonitrile given in Figure 5. It is also observed for multivalent electrolytes in high permittivity solvents, such as water. The additional relaxation process is the manifestation of strong ion–ion interactions leading to the formation of dipolar aggregates which are stable in the time scale of the experiment, *i.e.* for several pico- to nano-seconds.

The solute relaxation processes studied in our laboratory[14,22] in the solvents water, methanol, acetonitrile, DMSO, and DMF, are all due to ion-pair formation

$$C^{z+} + A^{z-} \underset{k_{21}}{\overset{k_{12}}{\rightleftharpoons}} IP^{z+ \; z-} \quad (24)$$

governed by the equilibrium constant $K_A = k_{12}/k_{21}$; k_{12} and k_{21} are the rate constants of ion-pair formation and decomposition, respectively. It is possible to determine the concentration of the ion pairs in the solution, c_{IP}, from the solute dispersion amplitude $(\epsilon - \epsilon_s)$ with the help of dipole moments μ_{IP} calculated on the base of appropriate models.[28]

$$c_{IP} = \frac{2\epsilon + 1}{3\epsilon} \cdot \frac{3kT\epsilon_0}{10^{-3} N_A} \cdot \frac{(1 - \alpha_{IP} f_{IP})^2}{\mu^2_{IP}} \cdot (\epsilon - \epsilon_s) \quad (25)$$

In equation 25 α_{IP} is the polarizability and f_{IP} is the reaction field factor of the ion pair. From the c_{IP}-data association constants K_A can be estimated. Static methods, like calorimetry, vapour pressure or electromotoric force measurements, and especially conductance studies yield comparable values of K_A, but are less suited to inform about the structure of the ion pair. However, the combination of these data with dielectric relaxation results permits the unambiguous identification of contact (CIP) and solvent-shared (SSIP) ion pairs, see Table 2. Dielectric relaxation experiments even yield detailed information on ion-pairing for systems with low association constants such as $NaClO_4$ in DMF or complex-forming asymmetric electrolytes, like $CdCl_2$ in water.[24] Such solutions are difficult to assess by other techniques.

The ion-pair relaxation time τ_{IP} is a source of further information. For the studied systems the values typically are around 100 to 200 ps and one intuitively would expect that the microscopic relaxation time τ'_{IP} follows the SED-equation (8). For some systems, such a behaviour is observed. However, more often a minimum of the relaxation time is found in the τ_{IP} *vs.* η plot, indicating that the ion aggregates cannot be stable particles in the time-scale of the dielectric relaxation experiment.

The superimposition of ion-pair rotational diffusion, controlled by the correlation time τ'_{IP}, and chemical equilibrium, equation 25, governed by the ion-pair formation and decomposition rate constants k_{12} and k_{21} yields an ion-pair relaxation rate τ_{IP}^{-1} which is proportional to the concentration of free ions, $c - c_{IP}$[29]

$$\tau_{IP}^{-1} = (\tau'_{IP})^{-1} + k_{21} + 2k_{12}(c - c_{IP}) \quad (26)$$

This equation is followed up to the relaxation time minimum. It permits the determination of the rate constant of ion-pair formation, k_{12}, from the slope of the diagram τ_{IP}^{-1} *vs.* $(c - c_{IP})$. The rate constant of the decomposition process then is calculable from the association constant, $k_{21} = k_{12}/K_A$, and permits the determination of the ion-pair rotational correlation time τ'_{IP}. The latter quantity can be compared with the SED-equation (8). The type of ion-pair compatible with the dispersion amplitudes is generally corroborated.

Table 2 summarizes some rate constants obtained from dielectric relaxation data. The rate constants of formation k_{12} are in the order of 10^9—10^{10} $dm^3\,mol^{-1}\,s^{-1}$, whereas k_{21} varies between 10^7 s^{-1} and 10^9 s^{-1}. The corresponding chemical relaxation time τ_{ch}, $\tau_{ch}^{-1} = k_{21} + 2k_{12}(c - c_{IP})$, is of the order of 100 ps. This range is scarcely accessible by other methods; even faster reactions can be studied by dielectric methods. With the exception of $NaClO_4$ in DMF, the formation rate constants obtained for ion-pair formation are about a factor of 10 smaller than those expected for a diffusion-controlled reaction, suggesting that non-coulombic interactions – possibly desolvation processes – are of prime importance in ion-pair formation.

Obviously, equation 26 does not explain the increase of τ_{IP} at higher concentrations. This statement is not significantly changed by the consideration of the viscosity dependence of the rotational correlation time τ'_{IP}.[24] Possibly this phenomenon is due to the formation of higher ion aggregates, but again further information is needed for a conclusive decision.

6 References

1 J. Burgess, 'Ions in Solution', Ellis Horwood, Chichester, 1988.
2 Y. Marcus, 'Ion Solvation', Wiley, Chichester, 1985.
3 'The Physics and Chemistry of Aqueous Ionic Solutions', ed. M. C. Bellissent-Funel and G. W. Neilson, NATO ASI Series, Series C, Vol. 205, Reidel, Dordrecht, 1987.

Table 2 Association and rate constants of ion-pair formation from dielectric relaxation data at 25 °C (From reference 14)

Solvent	Electrolyte	IP	K_A	$K_A^{lit.}$	$k_{12} \cdot 10^{-9}$	$k_{21} \cdot 10^{-7}$
			$dm^3 mol^{-1}$		$dm^3 mol^{-1} s^{-1}$	s^{-1}
water	$MgSO_4$	SSIP	164 ± 25	156	1.8 ± 0.1	1.1 ± 0.1
	$CdSO_4$	SSIP	270 ± 90	245	2.3 ± 0.4	0.9 ± 0.2
acetonitrile	LiBr	CIP	148 ± 2	155—193		*a*
	NaI	CIP	17 ± 6	3.8—24	8 ± 1	0.4 ± 0.1
	$NaClO_4$	CIP	31 ± 3	15—27	10.7 ± 0.4	0.44 ± 0.04
DMF	$NaClO_4$	SSIP	1.9 ± 1.3	3.2 ± 0.7	4.7 ± 0.2	1.5 ± 0.3

$K_A^{lit.}$ from conductance or calorimetric data; [a] τ_{IP} constant

4 H. L. Friedman, *Faraday Discuss. R. Soc. Chem.*, 1988, **85**, 1.
5 W. Kunz, P. Turq, and J. Barthel, *Ann. Phys. Fr.*, 1990, **15**, 447.
6 A. K. Jonscher, 'Dielectric Relaxation in Solids', Chelsea Dielectric Press, London, 1983.
7 C. C. Ku and R. Liepins, 'Electrical Properties of Polymers', Hanser, Munich, 1987.
8 L. M. Blinov, 'Electro-optical and Magneto-optical Properties of Liquid Crystals', Wiley, Chichester, 1983.
9 E. H. Grant, R. J. Sheppard, and G. P. South, 'Dielectric Behaviour of Biological Molecules in Solution', Clarendon, Oxford, 1978.
10 (*a*) C. F. J. Böttcher, 'Theory of Dielectric Polarization', Vol. 1 (2nd ed.), Elsevier, Amsterdam, 1973; (*b*) C. F. J. Böttcher and P. Bordewijk, 'Theory of Dielectric Polarization', Vol. 2 (2nd ed.), Elsevier, Amsterdam, 1978.
11 H. J. Kim, H. L. Friedman, and F. O. Raineri, *J. Chem. Phys.*, 1991, **94**, 1442.
12 J. C. Dote, D. Kivelson, and R. N. Schwartz, *J. Phys. Chem.*, 1981, **85**, 2169.
13 M. W. Evans, G. J. Evans, W. T. Coffey, and P. Grigolini, 'Molecular Dynamics', Wiley, Chichester, 1982.
14 J. Barthel, K. Bachhuber, R. Buchner, H. Hetzenauer, M. Kleebauer, and H. Ortmaier, *Pure Appl. Chem.*, 1990, **62**, 2287.
15 L. A. Dissado and R. M. Hill, *Proc. R. Soc. London*, 1983, **A 390**, 131.
16 J. Barthel, K. Bachhuber, R. Buchner, H. Hetzenauer, and M. Kleebauer, *Ber. Bunsenges. Phys. Chem.*, 1991, **95**, 853.
17 (*a*) J. M. Alison and R. J. Sheppard, *Meas. Sci. Technol.*, 1990, **1**, 1093; (*b*) M. G. Richards and R. J. Sheppard, *ibid.*, 1991, **2**, 663.
18 D. Steele and J. Yarwood, 'Spectroscopy and Relaxation of Molecular Liquids', Elsevier, Amsterdam, 1991.
19 T. Ohba and S. Ikawa, *Mol. Phys.*, 1991, **73**, 985.
20 Y.-Z. Wei and S. Sridhar, *Rev. Sci Instrum.*, 1989, **60**, 3041.
21 D. Bertolini, M. Cassetari, G. Salvetti, E. Tombari, and S. Veronesi, *Rev. Sci. Instrum.*, 1990, **61**, 450.
22 J. Barthel and R. Buchner, *Pure Appl. Chem.*, 1991, **63**, 1473.
23 J. B. Hubbard, P. Colonomos, and P. G. Wolynes, *J. Chem. Phys.*, 1979, **71**, 2652.
24 J. Barthel, H. Hetzenauer, and R. Buchner, *Ber. Bunsenges. Phys. Chem.*, (*a*) 1992, **96**, 988; (*b*) in press.
25 R. Buchner and J. Barthel, *J. Mol. Liq.*, 1992, **52**, 13.
26 B. Bagchi, *Annu. Rev. Phys. Chem.*, 1989, **40**, 115.
27 P. F. Barbara and W. Jarzeba, *Adv. Photochem.*, 1990, **15**, 1.
28 E. A. S. Cavell, P. C. Knight, and M. A. Sheikh, *J. Chem. Soc., Faraday Trans.*, 1972, **67**, 2225.
29 R. Buchner and J. Barthel, *J. Mol. Liq.*, in press.